nature geoscience

Article

https://doi.org/10.1038/s41561-025-01873-3

Underestimation of particulate dry nitrogen deposition in China

Received: 11 July 2024

Accepted: 4 November 2025

Published online: 02 January 2026

Check for updates

Qianru Zhang[1,2,3], Yuhang Wang[3] ✉, Maodian Liu[1,4] ✉, Young-Hee Ryu[5], Mingxu Liu[6], Huoqing Li[7], Si-Yi Wei[2,8,9], Junfeng Liu[1], Shu Tao[1] & Xuejun Wang[1,10] ✉

Nitrogen is indispensable for global food production and ecosystem carbon sequestration, but excess nitrogen leads to water eutrophication, soil acidification and air pollution. Atmospheric nitrogen deposition is a key yet uncertain component of the biogeochemical cycle. Currently, global networks monitoring particulate nitrogen dry deposition rely mainly on measured concentrations and modelled dry deposition velocities, which remain poorly constrained. Here we develop a spatially explicit dataset by integrating observation-constrained size distribution and dry deposition mechanisms to re-evaluate atmospheric nitrogen deposition across China. We reveal that atmospheric chemistry models underestimate the particle size of fine-mode nitrogen-containing aerosols in China by more than twofold. Additionally, dry particle deposition velocity estimates with different mechanisms diverge by up to two orders of magnitude. Our corrections indicate that atmospheric chemistry models and China's observation network underestimate particulate nitrogen dry deposition by 2–5 times. Furthermore, most Earth system models underestimate particulate dry deposition of ammonium, a major nitrogen species, by 31%–98%. By integrating these corrections into the Community Land Model, we demonstrate that the effect of nitrogen deposition on China's terrestrial net ecosystem productivity may have been underestimated by 9%–13%. As China contributes nearly 20% of global nitrogen deposition, its impact on terrestrial carbon sinks and ecosystem health could be greater than previously recognized.

Nitrogen, a fundamental element of living organisms, plays a vital role in Earth's biogeochemistry[1]. Imbalances in the global nitrogen cycle can negatively affect ecosystem health[2]. Reactive nitrogen (Nr) species in the atmosphere, including inorganic oxidized and reduced forms and organic compounds, are important for their biological, photochemical and radiative activities[3]. The global atmospheric Nr reservoir comprises both particulate (for example, NO_3^-, NH_4^+) and gaseous species (for example, NO_2, NH_3, HNO_3)[3]. These primary pollutants or secondary atmospheric products contribute to secondary pollutant formation, impacting air quality and public health[4]. Furthermore, atmospheric Nr deposition, a key component of global Nr cycling, has tripled since industrialization[5], affecting ecosystem health[4,6], such as reduced biodiversity[7], soil acidification[8], water eutrophication[9] and shifts in biogeochemical cycles, particularly carbon[10,11]. By alleviating nitrogen limitation[10], atmospheric Nr deposition stimulates photosynthesis and adds up to 0.3 PgC yr^{-1} to global land sinks[12,13], helping lower atmospheric CO_2[11].

Atmospheric Nr deposition is a major source of uncertainty in understanding the global nitrogen cycle[14–16]. The deposition primarily occurs through wet and dry processes. Whereas wet Nr deposition can

A full list of affiliations appears at the end of the paper. e-mail: ywang@eas.gatech.edu; maodian.liu@pku.edu.cn; xjwang@urban.pku.edu.cn

https://doi.org/10.1038/s41561-025-01873-3

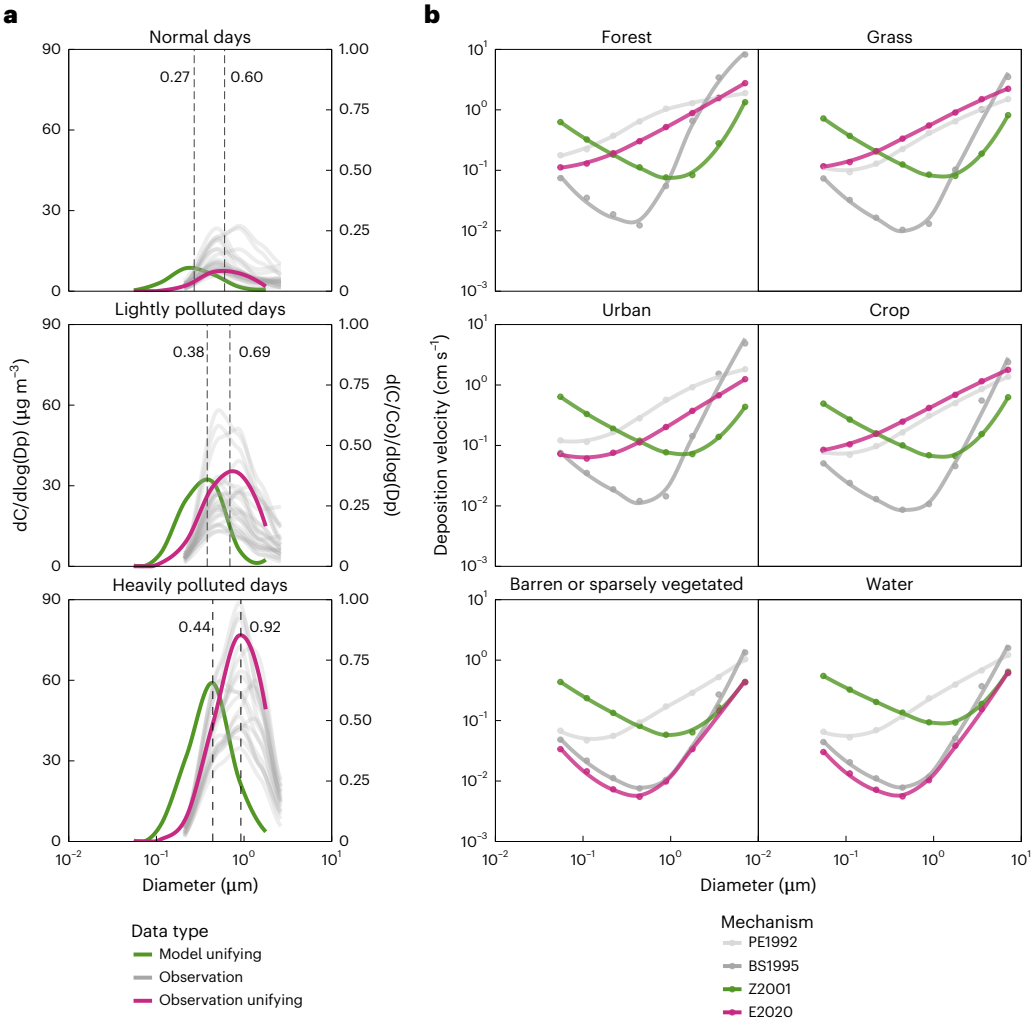

Fig. 1 | Key factors affecting particulate nitrogen dry deposition. a, Model default and observed particle size distributions of NO_3^-, NH_4^+ and SO_4^{2-} aerosols under three air pollution conditions in China. Green lines are simulated by the default model, grey lines are the observation data in spring, summer, autumn and winter in two urban sites in China, and pink lines are the result of unifying all observed data. To align with the observations employed, the green lines were averaged from simulations conducted for the spring (April), summer (July), autumn (October) and winter (January) seasons within the grid cells where the Beijing and Tianjin stations are located. The modeled (green) and observed (grey) distributions use the left *y* axis, where dC/dlog(Dp) indicates the aerosol mass concentration per logarithmic particle diameter interval. The pink lines, based on observational data, use the right *y* axis, where d(C/Co)/dlog(Dp) denotes the normalized aerosol mass concentration per logarithmic particle diameter interval. The black dashed lines and the numbers marked in the figure are the particle sizes corresponding to the peaks of the particle size distribution. **b**, Variation of particle dry deposition velocity with particle diameter for different land-use cover types calculated by four schemes in the atmospheric chemistry model in China. The values were averaged from the spring (April), summer (July), autumn (October) and winter (January) seasons. Four different colours represent four different particle dry deposition mechanisms. The land-use types are defined in Supplementary Table 4 and Supplementary Fig. 4.

be extrapolated from in situ measurements, estimating dry deposition at regional to global scales is challenging[14]. This estimation typically involves combining in situ observations or satellite-derived ambient Nr concentrations with modelled deposition velocities for particulate and gaseous Nr species using process-based models such as Chemical Transport Models (CTMs) and Earth System Models (ESMs) or directly obtaining it from these models' simulations[14,16,17]. Key monitoring networks such as the Canadian Air and Precipitation Network, US Clean Air Status and Trends Network, the NitroEurope network, Acid Deposition Monitoring Network in East Asia (EANET) and China's Nationwide Nitrogen Deposition Monitoring Network (NNDMN) utilize this inferential approach for estimating dry deposition[14,18–20]. The accuracy of these networks relies heavily on the simulated dry deposition velocity, which is strongly influenced by particle size distributions and the parameterization of size-resolved dry deposition.

However, large uncertainties remain in simulating particle sizes within atmospheric models, particularly in China, where pollution levels are high. As a global hotspot for atmospheric Nr deposition[21], China's terrestrial Nr deposition rates are estimated to be ~7 times higher than the global average[22]. Observations show that surface air particles in China primarily exhibit an accumulation mode with a modal size of 0.6–1.4 μm (refs. 23–25) (specifically referring to inorganic nitrogen-containing aerosols), which is approximately a factor of two larger than the modal size observed in North America[26–29]. However, particle size distributions in process-based models are mostly based on observations from North America and surrounding marine areas[26,30]. Because larger particles tend to have higher dry deposition velocities, current models probably underestimate particulate Nr deposition in China.

Furthermore, recent research has highlighted uncertainties in the particle dry deposition mechanisms commonly used in models[16,31]. Emerson et al. introduced an observation-constrained deposition mechanism that revealed previous parameterizations overestimated dry deposition for fine-mode particles but underestimated it for

https://doi.org/10.1038/s41561-025-01873-3

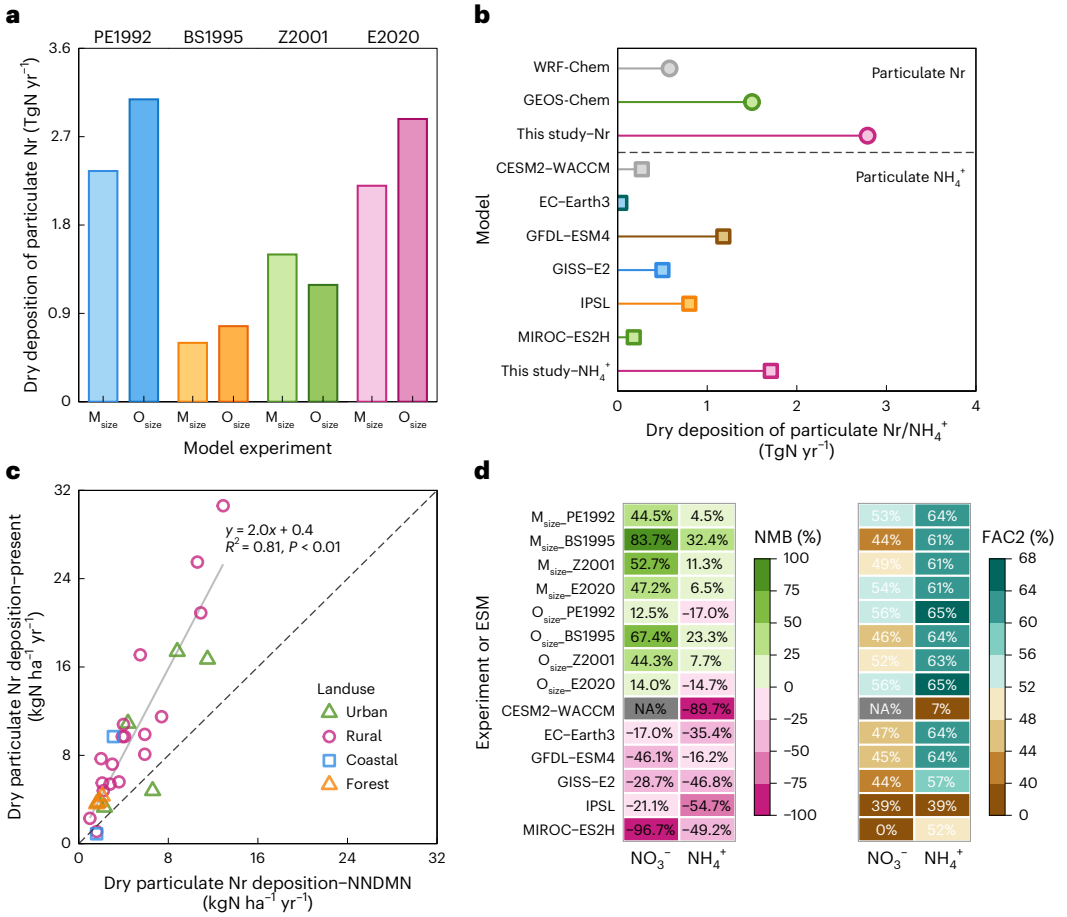

Fig. 2 | Particulate nitrogen dry deposition flux in China. a, Comparison of the atmospheric particulate nitrogen dry deposition in China under eight different model experiments in 2015. **b**, Comparison of observation-constrained dry deposition of particulate nitrogen in this study with that obtained from different ESMs and WRF-Chem and GEOS-Chem default models. Because ESM outputs lack data on particulate NO_3^- dry deposition, only comparisons of particulate NH_4^+ dry deposition are presented here. **c**, Comparison of particulate nitrogen deposition at nitrogen deposition monitoring sites in 2015, based on observation-constrained dry deposition velocities from this study and concentrations from published literature[18], with the original deposition data from the same study[18]. **d**, The statistical results for comparison of simulated and observed NO_3^- and NH_4^+ concentration values under eight different experiments, along with the statistical values from ESMs. NMB stands for normalized mean bias, and FAC2 represents the fraction of simulations within a factor of two. FAC2 is calculated as the proportion of data points where the ratio of simulated to observed values falls within the range of 0.5 to 2. The observed data were obtained from the nationwide nitrogen deposition monitoring network in China and published literature (Supplementary Fig. 5).

coarse-mode particles[31]. However, this new mechanism has not been applied to observation-constrained particle size distributions in polluted regions such as China, where particle sizes tend to larger[32,33]. Consequently, Nr deposition in China remains poorly constrained, introducing substantial uncertainties in our understanding of the nitrogen cycle. These uncertainties hinder our ability to accurately predict the impacts of Nr pollution and to develop effective regulatory targets for Nr pollution control.

We hypothesize that the poorly constrained particle size distributions of nitrogen-containing aerosols and the mechanisms of particle dry deposition greatly impact the accuracy of Nr deposition quantification in China. Addressing this issue is urgently needed, given that ambient air pollution in China contributes to over 1 million premature deaths annually[34], and Nr deposition influences the composition and lifetime of aerosols, affecting air quality and human health[4,35,36]. Furthermore, China's terrestrial ecosystems, representing approximately 5%–10% of annual terrestrial carbon sinks worldwide[37,38], are closely related to Nr deposition.

In this study, we leveraged the growing availability of observed particle size distribution data in China, combined with four commonly used particle dry deposition mechanisms (Extended Data Table 1), to examine their spatio-temporal effects on Nr deposition using the Weather Research and Forecasting Model coupled to Chemistry (WRF-Chem), a widely used atmospheric model. By integrating observed aerosol particle size constraints and identifying the deposition mechanism that best reflects China's pollution dynamics, we developed a spatially detailed dataset to reassess atmospheric Nr deposition across the country and tested its robustness against observations. Furthermore, we highlight the implications of corrected Nr deposition estimates for understanding terrestrial carbon sequestration. Our findings provide valuable insights into the continental-scale nitrogen cycle and improve the predictions of air pollution and climate change impacts.

Importance of particle size and dry deposition mechanisms

Our analysis reveals that standard models substantially underestimate the particle size of inorganic Nr particles across China compared to observations. Specifically, in the models, the simulated peaks of the particle size distribution are consistently lower than the observations in Beijing and Tianjin by factors of two to three (Fig. 1a). These cities were chosen for comparison due to their observations spanning a range of pollution conditions, covering normal, lightly polluted and heavily polluted days across all seasons. We also extended this comparison to include observations from eight other studies across

China. Whereas these datasets are less comprehensive than those from Beijing and Tianjin (Supplementary Table 1), they consistently indicate a systematic underestimation of the sizes of Nr particles by the model (Extended Data Fig. 1). Given the limited understanding of the mechanisms controlling aerosol particle size[39], we employed an observation-constrained approach (Methods: 'Particle size distribution') in subsequent analyses to more accurately assess the impact of particle size on Nr deposition.

We observe substantial discrepancies in particle deposition velocities across different dry deposition mechanisms. We ran eight experiments to characterize the uncertainty in simulating particulate dry deposition: four with observation-based particle size distributions (O_{size} series) and four with default particle sizes (M_{size} series). These experiments focused on NO_3^- and NH_4^+, key Nr components in atmospheric particles[40]. Each set paired one of four resistance-based schemes, that is, 'PE1992'[41], 'BS1995'[42], 'Z2001'[43] and the newest observation-driven 'E2020'[31] (Methods: 'Aerosol dry deposition mechanisms'). PE1992, once used in early WRF-Chem, is now rarely applied; BS1995 is widely used in the current version, whereas Z2001 is common in models such as GEOS-Chem, CAMx and many ESMs. E2020 is the most recent and observation-constrained mechanism but remains underutilized.

We find that the discrepancies among these mechanisms are evident in two key aspects: (1) for different surface types, each mechanism's deposition velocities exhibit distinct 'U'-shaped curves, with the lowest point of each curve corresponding to noticeably different diameters (Fig. 1b). (2) In the accumulation mode of particles (0.05–2 µm, where particles are concentrated), the deposition velocities calculated by different mechanisms show considerable variations (Fig. 1b). A detailed comparison of these four mechanisms is presented in Supplementary Text 1. In the following sections, we further analyse the performance of these mechanisms and find that E2020 most accurately represents atmospheric Nr deposition and nitrate pollution in China.

Underestimation of particulate dry nitrogen deposition across China

Our findings highlight that most current models greatly underestimate particulate Nr dry deposition across China. Among eight experiments, annual deposition spans 0.60–3.1 TgN yr^{-1} (Fig. 2a), with up to fourfold discrepancies between different particle dry deposition mechanisms. Switching from model-based to observation-constrained particle size distributions caused further variations within the same mechanism (−21% to +31%). These divergences reflect the differences in the particle diameters at which each scheme's characteristic 'U-shaped' velocity curves reach their minimum (Fig. 1 and Supplementary Text 2). Furthermore, the observation-constrained experiment with the newest E2020 parameterization (O_{size}_E2020) gives a deposition flux of 2.9 TgN yr^{-1} (Fig. 2a), whereas the standard WRF-Chem setup (M_{size}_BS1995) yields only 0.60 TgN yr^{-1}. A GEOS-Chem value of 1.5 TgN yr^{-1} (ref. 44), mirrored by M_{size}_Z2001 (1.5 TgN yr^{-1}; Fig. 2a), falls midway. Thus, conventional CTMs underestimated China's dry deposition of particulate Nr by a factor of 2–5, with the largest shortfall in Nr emissions-intensive eastern China (Extended Data Fig. 2).

Although total particulate Nr dry deposition fluxes from PE1992 and E2020 are similar for China (Fig. 2a), their spatial distributions show substantial differences (Extended Data Fig. 2). This discrepancy stems primarily from the influence of surface physical characteristics on particulate dry deposition velocities for different land-use types[31,45,46]. Whereas PE1992 is based on spruce forest observations only, which were extrapolated to other land types, E2020 explicitly accounts for the dependence of particulate dry deposition on land-use type. In China, Nr deposition is concentrated in forested and northern agricultural areas. Derived exclusively from spruce forest data, PE1992 overestimates Nr deposition in eastern forests and the western barren region, while underestimating it over northern farmland; these opposing biases cancel out in the national total, masking its substantial inaccuracy relative to E2020 (Extended Data Fig. 2). By integrating multi-surface observations, E2020 performs robustly across land-cover types[31], and its velocity estimates over flat terrains such as deserts and water bodies (Fig. 1b) align closely with recent observational data[31,46]. Thus, neglecting the improvements made in land-use type representation in E2020 introduces considerable biases in estimating Nr deposition distribution across China.

Furthermore, our analysis highlights a persistent trend in ESMs underestimating the dry deposition of particulate NH_4^+. Comparing Coupled Model Intercomparison Project Phase 6 (CMIP6) historical simulations with our observation-constrained estimates, we find that the deposition values derived from ESMs are 31%–98% lower (Fig. 2b). Beyond differences in dry deposition mechanisms, uncertainties are further amplified by the oversimplification of atmospheric processes in ESMs, particularly regarding aerosols and chemistry schemes[47]. This comparison focuses solely on NH_4^+ due to the absence of separate NO_3^- deposition data in the CMIP6 dataset.

The observation-based NNDMN dataset in China is of great importance for understanding nitrogen cycling both locally and globally[48,49]. However, our analysis reveals that NNDMN has underestimated particulate Nr dry deposition in China. In the NNDMN, particulate Nr dry deposition was calculated by integrating particle dry deposition velocities simulated by GEOS-Chem with ground-level measurements of NO_3^- and NH_4^+ concentrations from 32 monitoring sites across China[18]. Thus, this underestimation is primarily attributed to GEOS-Chem's use of the Z2001 dry deposition mechanism (Fig. 2a)[18]. By incorporating our observation-constrained particle size distribution and dry deposition mechanism[31], we update the 2015 particulate dry Nr deposition estimates for NNDMN, showing a twofold increase compared to the original data (Fig. 2c)[18]. Together, particulate nitrogen dry deposition across China is far larger and far more uneven than current models and observation-based datasets suggest.

Improved prediction of nitrate aerosol concentrations

Accurate predictions of Nr concentrations are crucial for improving estimates of particulate Nr dry deposition fluxes and enhancing air quality forecasting. The persistent overestimation of atmospheric particulate NO_3^- concentration in China by many CTMs remains an unresolved issue[50,51]. Our study shows that integrating observation-constrained particle size distribution with the new E2020 particle dry deposition mechanism can greatly reduce this overestimation. Figure 2d compares simulated particulate NO_3^- concentrations across various experiments. We found that the normalized mean bias (NMB) for NO_3^- in the most commonly used mechanisms (M_{size}_BS1995 and M_{size}_Z2001) was as high as 84% and 53%, respectively. However, after applying observation constraints, the NMB decreased to 67% and 44% (O_{size}_BS1995 and O_{size}_Z2001), highlighting the importance of particle size constraints in NO_3^- concentration simulations. Under the O_{size}_PE1992 and O_{size}_E2020 mechanisms, the NMB dropped further to 13% and 14%, respectively, indicating that the BS1995 and Z2001 mechanisms largely overestimate aerosol NO_3^- concentrations in China. The fraction of simulation within a factor of two (FAC2) for NO_3^- varies from 44% to 56%. O_{size}_E2020 shows up to 12% improvement compared to other experiments (Fig. 2d). Note that FAC2 evaluates the proportion of simulated values within a twofold range of observed values, making it essential to further evaluate model accuracy using the NMB indicator.

Both PE1992 and E2020 mechanisms greatly improve the simulation of particulate NO_3^- concentration in China when particle size distributions are constrained by observations. However, PE1992 is based solely on observations in spruce forests and extrapolated to all other land-cover types[52], which introduces considerable uncertainties in dry deposition across diverse landscapes[31]. Furthermore, as an earlier mechanism, PE1992 has largely been replaced by the newer

https://doi.org/10.1038/s41561-025-01873-3

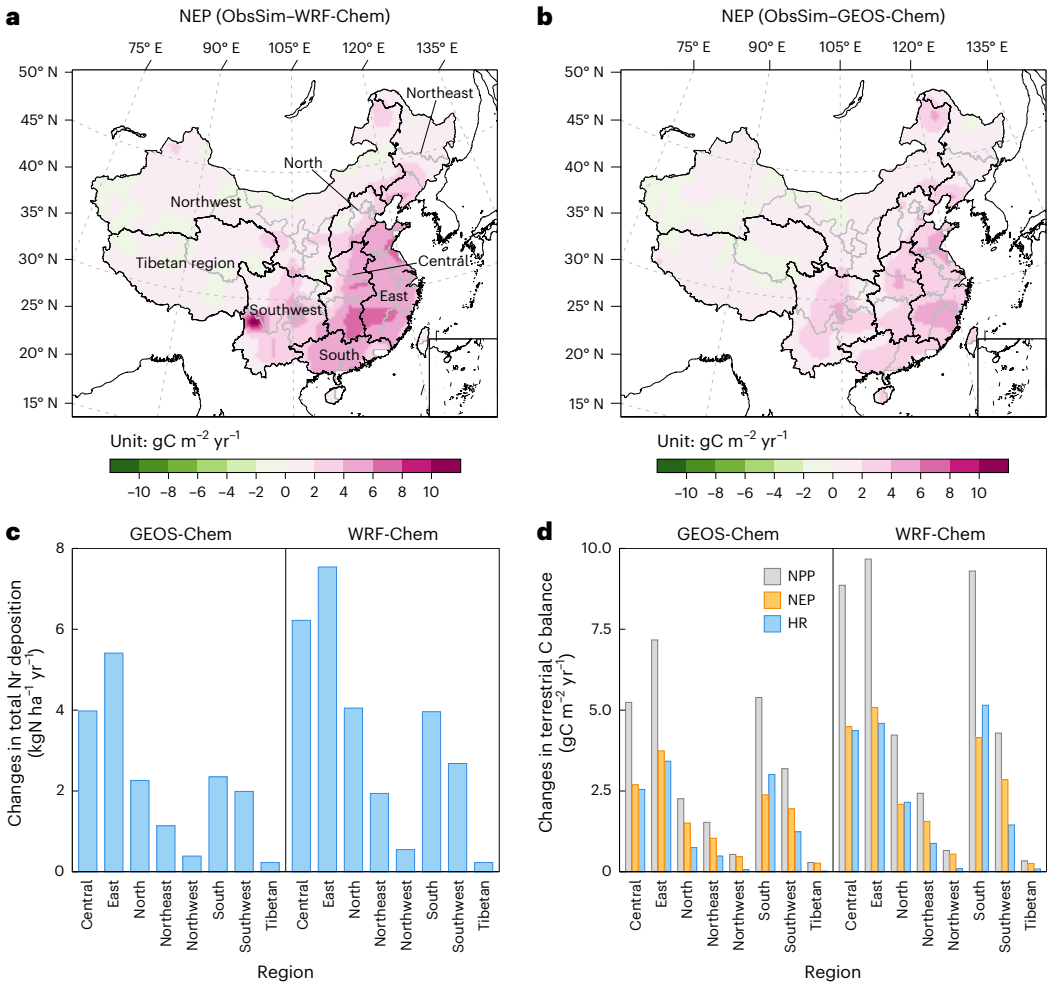

Fig. 3 | The impact of nitrogen deposition variation on the terrestrial carbon sink in China. a,**b**, The impact of changes in nitrogen deposition on NEP over China under observation-derived experiment (ObsSim) compared to the nitrogen deposition from WRF-Chem default (**a**) and GEOS-Chem default (**b**). Grey lines indicate provincial boundaries, and black lines delineate the eight regions used in the analysis. **c**, The impact of the observation-derived experiment on total nitrogen deposition across different regions in China, compared with two typical model experiments (WRF-Chem default and GEOS-Chem default). **d**, Re-evaluating the impact of nitrogen deposition on terrestrial carbon sinks in China. This panel demonstrates the impact of nitrogen deposition changes of the observation-derived experiment compared with two typical model experiments (WRF-Chem default and GEOS-Chem default) on terrestrial carbon balance (NPP, HR and NEP) in different regions in China. HR represents heterotrophic respiration. Maps based on the original NCAR Command Language (NCL) map framework with updated boundary information derived from the National Catalogue Service for Geographic Information of China (http://www.webmap.cn/commres.do?method=result100W).

BS1995 and Z2001. In contrast, E2020 provides a more comprehensive representation of various land-use types, improving its applicability for accurate Nr deposition modelling across different land surfaces. Therefore, E2020 is the preferable choice for Nr deposition modelling.

The simulation of particulate NH_4^+ concentration showed limited improvement in CTMs. The FAC2 values for NH_4^+ in all experiments remained 61%–65% and highest for O_{size}_PE1992 and O_{size}_E2020 (Fig. 2d). Most experiments overestimated NH_4^+ concentrations (NMB values between 4.5% and 32%), whereas O_{size}_PE1992 and O_{size}_E2020 slightly underpredicted them (NMB values of −17% and −14.7%, respectively; Fig. 2d). Accurate simulation of NH_4^+ is challenging, and an NMB value within ±30% has previously been considered acceptable[53,54]. The limited improvement is probably due to uncertainties in China's NH_3 emissions inventory, as highlighted by recent studies[55,56]. Our additional simulations show that increasing NH_3 emissions improves the NH_4^+ concentration simulation using the new E2020 mechanism (Supplementary Text 3), suggesting that improving NH_3 emissions inventories could be important to better NH_4^+ simulations.

We conducted sensitivity experiments to assess the impact of the limited improvement in NH_4^+ concentration simulation on our conclusion that particulate Nr dry deposition is substantially underestimated in China. These experiments revealed that, regardless of NH_3 emission levels, total particulate Nr deposition under the new mechanism (O_{size}_E2020) was approximately five times higher than under the default model (M_{size}_BS1995) (Supplementary Tables 2 and 3). This finding reinforces our hypothesis of the substantial particulate Nr dry deposition underestimation in China. Additionally, the simulation of wet NH_4^+ deposition using the new mechanism showed good agreement with observations (NMB and FAC2 of −20.6% and 82%, respectively (Supplementary Fig. 1), indicating its applicability to NH_4^+ wet deposition. Sensitivity tests also revealed that the new mechanism's total atmospheric Nr deposition is less sensitive to NH_3 emissions variations compared to the default mechanism (Supplementary Tables 2 and 3), suggesting greater robustness in deposition simulations. Thus, the limited improvement in NH_4^+ concentration simulation does not change the conclusion regarding the substantial underestimation of particulate Nr dry deposition in China.

However, our simulations of particulate NO_3^- and NH_4^+ concentrations show substantial improvements compared to those of ESMs. Among the six ESMs in Fig. 2b, which published simulated NO_3^- (five

models) and NH_4^+ (six models) concentrations, all of them underestimated the observed concentrations, with NMB ranging from −16% to −97% and average NMB of −42% and −49% for NO_3^- and NH_4^+, respectively (Fig. 2d). These deviations are larger compared to those for our study (Fig. 2d). In contrast to CTMs, many ESMs oversimplify atmospheric processes, resulting in inadequate representations of the atmospheric nitrogen cycle[57]. Our findings highlight the critical need to improve the representation of the atmospheric nitrogen cycle in ESMs to enhance the accuracy of Nr concentration and dry deposition simulations, which are essential for interdisciplinary climate studies.

Implications for nitrogen deposition and terrestrial carbon sinks

The reliability of atmospheric Nr deposition modelling is critical, as it directly affects air quality and carbon sink assessments, with important implications for public health and climate change projections[4,10]. Here we demonstrated that inadequate representation of particle size distribution causes a substantial underestimation of particulate dry Nr deposition across China. Moreover, the uncertainty surrounding particle dry deposition mechanisms further exacerbates the divergence in deposition estimates. Most models overlook the combined impacts of particle size distribution and dry deposition mechanisms, leading to considerable underestimation of particulate dry Nr deposition in China.

We evaluate the impact of our updated dry deposition of particulate Nr on the overall Nr deposition. Our updated modelling result demonstrates a notable increase (11%–18%) in China's total Nr deposition compared to standard model experiments (M_{size}_BS1995 and M_{size}_Z2001), which have been widely used in previous studies. The increase mainly occurs in eastern China (Extended Data Fig. 3). This suggests that ecological risks, such as soil acidification and biodiversity loss, may be more severe than previously recognized[58]. Seasonal analysis reveals a more pronounced increase in total Nr deposition during winter, coinciding with frequent haze events (Supplementary Fig. 2), implying a reduced contribution of Nr to haze formation[51]. Furthermore, the model shows a marked shift in the composition of Nr deposition (Supplementary Fig. 3), with the proportion of particulate Nr dry deposition in total Nr deposition increasing from 5%–12% to 20%, altering the dry-to-wet deposition ratio from 2:3 to nearly 1:1. This suggests that soils may accumulate more Nr during the dry season, reducing their nitrogen nutrient loss[59].

Our research highlights the importance of particulate dry Nr deposition in the terrestrial carbon cycle. By coupling the updated WRF-Chem with Community Land Model version 5 (CLM5), which well captures carbon fluxes (Extended Data Fig. 4), we demonstrate that underestimating particulate dry Nr deposition results in a 9%–13% underestimation of the impact of Nr deposition on China's terrestrial net ecosystem productivity (NEP, 11–16 TgC yr^{-1}; 1.2–1.7 gC m^{-2} yr^{-1}; Fig. 3a,b), with a corresponding 18–28 TgC yr^{-1} underestimation of net primary productivity (NPP). This discrepancy offsets CO_2 emissions from China's lakes and reservoirs (12 TgC yr^{-1}) (ref. 60) or rivals NPP gains from aerosol reductions under China's Clean Air Action Plan (20 TgC yr^{-1}) (ref. 61). Furthermore, this overlooked carbon sink matches global carbon fluxes from key processes[62,63], such as marine algal CO_2 sequestration (4–44 TgC yr^{-1}). Consequently, refining particle size and dry deposition velocity representations is critical for accurately evaluating terrestrial carbon uptake and national carbon budgeting.

Accurate estimates of atmospheric Nr deposition are crucial for reliable regional carbon sink assessments. We find that the underestimation of Nr deposition's impact on NEP is especially substantial in the East, Central and South regions (4.4, 3.6 and 3.3 gC m^{-2} yr^{-1}, respectively; Fig. 3c,d), twofold to threefold greater than the national average. These regions experience the largest shifts in atmospheric Nr input and contain extensive, nitrogen-limited natural vegetation (Supplementary Fig. 4)[64], making them especially responsive to additional Nr inputs that boost carbon sequestration. In the North region, deposition changes are comparable to those in the South region (3.2 vs 3.2 kgN ha^{-1} yr^{-1}; Fig. 3c), but cropland fertilization already supplies ample Nr[65], keeping the NEP response to just 1.8 gC m^{-2} yr^{-1} (Fig. 3d). Correcting this spatial bias is therefore essential for robust regional carbon-budget projections.

The uncertainties in this study primarily stem from the simulations of atmospheric Nr deposition and terrestrial carbon sinks. Although we conducted a detailed analysis of aerosol particle size distributions in multiple regions of China, ensuring the applicability of the observations, limitations in data availability still contribute to uncertainty. More broadly, investigations of aerosol particle size distributions in many regions remain relatively insufficient. Whereas we have made progress in improving CTM simulations of particulate NO_3^-, some underestimation of NH_4^+ remains. Previous studies have highlighted the large uncertainties in China's NH_3 emissions inventories, which directly affect atmospheric NH_4^+ simulations. Future improvements in NH_4^+ simulations may focus on enhancing the accuracy of the NH_3 emissions inventory. Additionally, differences in spatial resolution between WRF-Chem and CLM, along with their treatment of land covers, may affect model coupling. Finally, uncertainties in CLM's handling of land-management practices, such as nitrogen fertilization, could affect terrestrial carbon sink assessments. Besides nitrogen deposition, NEP estimates are also affected by other factors such as climate and CO_2 concentration[66], which may introduce additional uncertainties. As more measurements and improved statistical methods emerge, updating these estimates will be essential.

Finally, the larger deposition flux suggests that achieving China's ambitious ecosystem carbon sequestration goals may be more challenging than expected. With China's strategic plan to reduce pollution emissions, a substantial decrease in atmospheric Nr deposition is anticipated in the coming decades[48,67]. The strictest Nr reduction scenario projects a 65% decrease in emissions by the 2050s[68]. Considering only future emissions changes, assuming all other conditions remain constant, and incorporating WRF-Chem results along with the relationship between changes in anthropogenic emissions and nitrogen deposition[67], CLM implies that this reduction could cumulatively decrease China's NEP by 1,400 TgC by 2050. This reinforces the long-held concern that while controlling Nr pollution is vital, it may weaken terrestrial carbon sinks, potentially exacerbating global warming throughout the twenty-first century. Reducing greenhouse gas emissions is essential to balance the environmental feedback loops and mitigate climate change impacts.

Online content

Any methods, additional references, Nature Portfolio reporting summaries, source data, extended data, supplementary information, acknowledgements, peer review information; details of author contributions and competing interests; and statements of data and code availability are available at https://doi.org/10.1038/s41561-025-01873-3.

References

1. Gruber, N. & Galloway, J. N. An Earth-system perspective of the global nitrogen cycle. *Nature* **451**, 293–296 (2008).
2. Houlton, B. Z. et al. A world of cobenefits: solving the global nitrogen challenge. *Earth' s Future* **7**, 865–872 (2019).
3. Galloway, J. N. et al. Nitrogen cycles: past, present, and future. *Biogeochemistry* **70**, 153–226 (2004).
4. Pan, D. et al. Regime shift in secondary inorganic aerosol formation and nitrogen deposition in the rural United States. *Nat. Geosci.* **17**, 617–623 (2024).
5. Lamarque, J.-F. et al. Multi-model mean nitrogen and sulfur deposition from the Atmospheric Chemistry and Climate Model Intercomparison Project (ACCMIP): evaluation of historical and projected future changes. *Atmos. Chem. Phys.* **13**, 7997–8018 (2013).

6. Liu, X. J. et al. Enhanced nitrogen deposition over China. *Nature* **494**, 459–462 (2013).
7. Clark, C. M. & Tilman, D. Loss of plant species after chronic low-level nitrogen deposition to prairie grasslands. *Nature* **451**, 712–715 (2008).
8. Lu, X., Mao, Q., Gilliam, F. S., Luo, Y. & Mo, J. Nitrogen deposition contributes to soil acidification in tropical ecosystems. *Glob. Change Biol.* **20**, 3790–3801 (2014).
9. Maúre, E.dR., Terauchi, G., Ishizaka, J., Clinton, N. & DeWitt, M. Globally consistent assessment of coastal eutrophication. *Nat. Commun.* **12**, 6142 (2021).
10. Reay, D. S., Dentener, F., Smith, P., Grace, J. & Feely, R. A. Global nitrogen deposition and carbon sinks. *Nat. Geosci.* **1**, 430–437 (2008).
11. Lu, X. et al. Nitrogen deposition accelerates soil carbon sequestration in tropical forests. *Proc. Natl Acad. Sci. USA* **118**, e2020790118 (2021).
12. Gong, C. et al. Global net climate effects of anthropogenic reactive nitrogen. *Nature* **632**, 557–563 (2024).
13. Wang, R. et al. Global forest carbon uptake due to nitrogen and phosphorus deposition from 1850 to 2100. *Glob. Change Biol.* **23**, 4854–4872 (2017).
14. Zhang, Q. et al. Atmospheric nitrogen deposition: a review of quantification methods and its spatial pattern derived from the global monitoring networks. *Ecotoxilcol. Environ. Saf.* **216**, 112180 (2021).
15. Baker, A. R. et al. Observation- and model-based estimates of particulate dry nitrogen deposition to the oceans. *Atmos. Chem. Phys.* **17**, 8189–8210 (2017).
16. Saylor, R. D. et al. The particle dry deposition component of total deposition from air quality models: right, wrong or uncertain?. *Tellus Ser. B* **71**, 1550324 (2019).
17. Zhang, Y. et al. Long-term trends in total inorganic nitrogen and sulfur deposition in the US from 1990 to 2010. *Atmos. Chem. Phys.* **18**, 9091–9106 (2018).
18. Xu, W., Zhang, L. & Liu, X. J. A database of atmospheric nitrogen concentration and deposition from the nationwide monitoring network in China. *Sci. Data* **6**, 51 (2019).
19. Schwede, D. B. & Lear, G. G. A novel hybrid approach for estimating total deposition in the United States. *Atmos. Environ.* **92**, 207–220 (2014).
20. Flechard, C. R. et al. Dry deposition of reactive nitrogen to European ecosystems: a comparison of inferential models across the NitroEurope network. *Atmos. Chem. Phys.* **11**, 2703–2728 (2011).
21. Yu, G. R. et al. Stabilization of atmospheric nitrogen deposition in China over the past decade. *Nat. Geosci.* **12**, 424–429 (2019).
22. Ackerman, D., Millet, D. B. & Chen, X. Global estimates of inorganic nitrogen deposition across four decades. *Glob. Biogeochem. Cycle* **33**, 100–107 (2019).
23. Li, Q. K., Yang, Z., Li, X. D., Ding, S. Y. & Du, F. Seasonal characteristics of sulfate and nitrate in size-segregated particles in ammonia-poor and -rich atmospheres in Chengdu, Southwest China. *Aerosol Air Qual. Res.* **19**, 2697–2706 (2019).
24. Ding, X. X. et al. Characteristics of size-resolved atmospheric inorganic and carbonaceous aerosols in urban Shanghai. *Atmos. Environ.* **167**, 625–641 (2017).
25. Li, X. R. et al. Characterization of the size-segregated water-soluble inorganic ions in the Jing-Jin-Ji urban agglomeration: spatial/temporal variability, size distribution and sources. *Atmos. Environ.* **77**, 250–259 (2013).
26. Nolte, C. G. et al. Evaluation of the Community Multiscale Air Quality (CMAQ) model v5.0 against size-resolved measurements of inorganic particle composition across sites in North America. *Geosci. Model Dev.* **8**, 2877–2892 (2015).
27. Kelly, J. T. et al. Simulating the phase partitioning of NH_3, HNO_3, and HCl with size-resolved particles over northern Colorado in winter. *Atmos. Environ.* **131**, 67–77 (2016).
28. Yao, X. H. & Zhang, L. Sulfate formation in atmospheric ultrafine particles at Canadian inland and coastal rural environments. *J. Geophys. Res.: Atmos.* **116**, D10202 (2011).
29. Cabada, J. C. et al. Mass size distributions and size resolved chemical composition of fine particulate matter at the Pittsburgh supersite. *Atmos. Environ.* **38**, 3127–3141 (2004).
30. Adams, P. J. & Seinfeld, J. H. Predicting global aerosol size distributions in general circulation models. *J. Geophys. Res.: Atmos.* **107**, AAC 4-1–AAC 4-23 (2002).
31. Emerson, E. W. et al. Revisiting particle dry deposition and its role in radiative effect estimates. *Proc. Natl Acad. Sci. USA* **117**, 26076–26082 (2020).
32. Zhang, Q. et al. Wintertime formation of large sulfate particles in China and implications for human health. *Environ. Sci. Technol.* **57**, 20010–20023 (2023).
33. Wu, T. & Boor, B. E. Urban aerosol size distributions: a global perspective. *Atmos. Chem. Phys.* **21**, 8883–8914 (2021).
34. Xiao, Q. et al. Tracking PM2.5 and O_3 pollution and the related health burden in China 2013–2020. *Environ. Sci. Technol.* **56**, 6922–6932 (2021).
35. Seinfeld, J. H. & Pandis, S. N. *Atmospheric Chemistry and Physics: From Air Pollution to Climate Change* (Wiley, 2016).
36. Zhai, S. X. et al. Control of particulate nitrate air pollution in China. *Nat. Geosci.* **14**, 389–395 (2021).
37. Piao, S., He, Y., Wang, X. & Chen, F. Estimation of China's terrestrial ecosystem carbon sink: methods, progress and prospects. *Sci. China Earth Sci.* **65**, 641–651 (2022).
38. The Intergovernmental Panel on Climate Change. *Climate Change 2021: The Physical Science Basis* (eds Masson-Delmotte, V. et al.) (Cambridge Univ. Press, 2021).
39. Zaveri, R. A., Easter, R. C., Fast, J. D. & Peters, L. K. Model for Simulating Aerosol Interactions and Chemistry (MOSAIC). *J. Geophys. Res.: Atmos.* **113**, D13204 (2008).
40. Xu, W. et al. Seasonal characterization of organic nitrogen in atmospheric aerosols using high resolution aerosol mass spectrometry in Beijing, China. *ACS Earth Space Chem.* **1**, 673–682 (2017).
41. Peters, K. & Eiden, R. Modeling the dry deposition velocity of aerosol–particles to a spruce forest. *Atmos. Environ. A* **26**, 2555–2564 (1992).
42. Binkowski, F. S. & Shankar, U. The regional particulate matter model .1. Model description and preliminary results. *J. Geophys. Res.: Atmos.* **100**, 26191–26209 (1995).
43. Zhang, L. M., Gong, S. L., Padro, J. & Barrie, L. A size-segregated particle dry deposition scheme for an atmospheric aerosol module. *Atmos. Environ.* **35**, 549–560 (2001).
44. Zhao, Y. H. et al. Atmospheric nitrogen deposition to China: a model analysis on nitrogen budget and critical load exceedance. *Atmos. Environ.* **153**, 32–40 (2017).
45. Farmer, D. K., Boedicker, E. K. & DeBolt, H. M. Dry deposition of atmospheric aerosols: approaches, observations, and mechanisms. *Annu. Rev. Phys. Chem.* **72**, 375–397 (2021).
46. Petroff, A. & Zhang, L. Development and validation of a size-resolved particle dry deposition scheme for application in aerosol transport models. *Geosci. Model Dev.* **3**, 753–769 (2010).
47. Turnock, S. T. et al. Historical and future changes in air pollutants from CMIP6 models. *Atmos. Chem. Phys.* **20**, 14547–14579 (2020).
48. Liu, L., Wen, Z., Liu, S., Zhang, X. & Liu, X. Decline in atmospheric nitrogen deposition in China between 2010 and 2020. *Nat. Geosci.* **17**, 733–736 (2024).

49. Zhu, J. et al. Changing patterns of global nitrogen deposition driven by socio-economic development. *Nat. Commun.* **16**, 46 (2025).
50. Chen, L. et al. MICS-Asia III: multi-model comparison and evaluation of aerosol over East Asia. *Atmos. Chem. Phys.* **19**, 11911–11937 (2019).
51. Xie, X. et al. Modeling particulate nitrate in China: current findings and future directions. *Environ. Int.* **166**, 107369 (2022).
52. Zeng, Y. et al. WRF-Chem v3.9 simulations of the East Asian dust storm in May 2017: modeling sensitivities to dust emission and dry deposition schemes. *Geosci. Model Dev.* **13**, 2125–2147 (2020).
53. Emery, C. et al. Recommendations on statistics and benchmarks to assess photochemical model performance. *J. Air Waste Manage. Assoc.* **67**, 582–598 (2017).
54. Huang, L. et al. Recommendations on benchmarks for numerical air quality model applications in China–part 1: PM 2.5 and chemical species. *Atmos. Chem. Phys.* **21**, 2725–2743 (2021).
55. Zhang, X. et al. Ammonia emissions may be substantially underestimated in China. *Environ. Sci. Technol.* **51**, 12089–12096 (2017).
56. Kong, L. et al. Improved inversion of monthly ammonia emissions in China based on the Chinese ammonia monitoring network and ensemble Kalman filter. *Environ. Sci. Technol.* **53**, 12529–12538 (2019).
57. Flato, G. M. Earth system models: an overview. *Wiley Interdiscip. Rev. Clim. Change* **2**, 783–800 (2011).
58. Galloway, J. N. et al. The nitrogen cascade. *Bioscience* **53**, 341–356 (2003).
59. Fenn, M. E. et al. Ecological effects of nitrogen deposition in the western United States. *Bioscience* **53**, 404–420 (2003).
60. Ran, L. S. et al. Substantial decrease in CO_2 emissions from Chinese inland waters due to global change. *Nat. Commun.* **12**, 1730 (2021).
61. Zhou, H. et al. Recovery of ecosystem productivity in China due to the Clean Air Action plan. *Nat. Geosci.* **17**, 1233–1239 (2024).
62. Filbee-Dexter, K. et al. Carbon export from seaweed forests to deep ocean sinks. *Nat. Geosci.* **17**, 552–559 (2024).
63. Campbell, A. D., Fatoyinbo, L., Goldberg, L. & Lagomasino, D. Global hotspots of salt marsh change and carbon emissions. *Nature* **612**, 701–706 (2022).
64. Liu, X. Y., Tai, A. P. K. & Fung, K. M. Responses of surface ozone to future agricultural ammonia emissions and subsequent nitrogen deposition through terrestrial ecosystem changes. *Atmos. Chem. Phys.* **21**, 17743–17758 (2021).
65. Shang, F. et al. Substantial nitrogen abatement accompanying decarbonization suppresses terrestrial carbon sinks in China. *Nat. Commun.* **15**, 7738 (2024).
66. Friedlingstein, P. et al. Global carbon budget 2021. *Earth Syst. Sci. Data* **14**, 1917–2005 (2022).
67. Zhu, H. et al. The response of nitrogen deposition in China to recent and future changes in anthropogenic emissions. *J. Geophys. Res.: Atmos.* **127**, e2022JD037437 (2022).
68. Dynamic Projection for Emission in China (DPEC) v1.2 emission inventory. *MEICModel* http://meicmodel.org.cn/?page_id=1918&lang=en (2023).

[1]Ministry of Education Laboratory of Earth Surface Processes, College of Urban and Environmental Sciences, Peking University, Beijing, China. [2]Nicholas School of the Environment, Duke University, Durham, NC, USA. [3]School of Earth and Atmospheric Sciences, Georgia Institute of Technology, Atlanta, GA, USA. [4]School of the Environment, Yale University, New Haven, CT, USA. [5]Department of Atmospheric Sciences, Yonsei University, Seoul, South Korea. [6]State Key Joint Laboratory of Environmental Simulation and Pollution Control, College of Environmental Sciences and Engineering, Peking University, Beijing, China. [7]Institute of Desert Meteorology, China Meteorological Administration, Urumqi, China. [8]Center for Energy and Environmental Policy Research, Beijing Institute of Technology, Beijing, China. [9]School of Management, Beijing Institute of Technology, Beijing, China. [10]Institute of Carbon Neutrality, Peking University, Beijing, China. ✉e-mail: ywang@eas.gatech.edu; maodian.liu@pku.edu.cn; xjwang@urban.pku.edu.cn

Methods

Observations

To validate the model's particulate NH_4^+ and NO_3^- concentration results and calculate the particulate dry deposition fluxes, we utilized surface particulate NH_4^+ and NO_3^- concentration data from NNDMN in China. NNDMN, a national-scale monitoring network, provides monthly average surface concentrations of major N-containing compounds and monthly accumulated dry and wet (bulk) deposition data of nitrogen species from 2010–2015 across 32 sites in China[18]. Similar to US Clean Air Status and Trends Network and National Atmospheric Deposition Program in the USA, NNDMN's wet deposition fluxes are monitored data, whereas dry deposition fluxes for gaseous and particulate species are derived from model-simulated deposition velocities (for example, GEOS-Chem) combined with measured Nr concentration. In this study, we specifically used NNDMN data from 2015 (Supplementary Fig. 5). When comparing the model-simulated particulate Nr concentration data, we excluded observational data from the Wuwei station due to its rapidly increasing NH_3 emissions in recent years[69], which are not accurately captured in the NH_3 emissions inventory. Furthermore, in China, there is a lot of monitoring data related to the chemical composition analysis of $PM_{2.5}$, providing additional nitrogen-containing aerosol concentration data to evaluate the model's performance. Here monthly average surface concentrations of NO_3^- and NH_4^+ in $PM_{2.5}$ aerosols were compiled from 102 sets of data, each set representing a different month at a different site, as reported in the published literature. These data, measured at 40 monitoring sites across China, are detailed in Supplementary Table 5 and Supplementary Fig. 5, with all measurements conducted in 2015. We also gathered observations from 2014 to evaluate the ESMs' outputs from CMIP6 historical simulations (Supplementary Table 6 and Supplementary Fig. 5), as most ESMs simulate data only up to that year.

To illustrate the characteristics of aerosol particle size distribution under varying pollution conditions in China and to constrain the model's simulated size distributions of NO_3^-, NH_4^+ and SO_4^{2-} aerosols, we sourced data from 13 previous studies on size-segregated aerosols during different levels of polluted days across China (Supplementary Table 1 and Supplementary Fig. 5). Observational data on size-segregated aerosols in China are sparse and limited. The sampling seasons, air pollution conditions classifications and designed cut-off sizes of samplers varied across different studies (Supplementary Table 1), making it impractical to use all observational data to constrain the model. However, these observations indicated similar particle size distribution properties across different Chinese cities, suggesting a degree of generality (Supplementary Text 4 and Extended Data Fig. 1). Thus, we applied detailed observations from Beijing and Tianjin[70,71], which had consistent standards for classifying air pollution conditions and particle sizes and included four seasons of long-term measurements, to refine the model's simulated particle size distribution of NO_3^-, NH_4^+ and SO_4^{2-} aerosols. Observations from all other sites were used for model verification (Extended Data Fig. 1). Following the National Ambient Air Quality Standard issued by the government and based on previous research[70,72], three air pollution conditions in China were defined based on daily atmospheric $PM_{2.5}$ concentrations: normal days ($PM_{2.5} < 75\ \mu g\ m^{-3}$), lightly polluted days ($75\ \mu g\ m^{-3} \le PM_{2.5} < 150\ \mu g\ m^{-3}$) and heavily polluted days ($PM_{2.5} > 150\ \mu g\ m^{-3}$).

The observed wet deposition data of NH_4^+ and NO_3^- in 2015 were obtained from EANET. The wet deposition data from NNDMN include both wet and a portion of dry deposition[18], resulting in values higher than actual wet deposition observations. Thus, we utilized observational data from EANET for a more accurate evaluation of the model's performance. Because not all EANET stations fall within our simulation area, we selected data from 24 stations located within our simulation domain (Supplementary Fig. 6) to evaluate the accuracy of the wet deposition simulated by the model.

Atmospheric chemical transport model configurations

We employed a regional high-resolution CTM, WRF-Chem model version 3.9, for simulating emissions, transport, chemical reactions and both dry and wet deposition of various Nr species (that is, NO, NO_2, HNO_3, NH_3, N_2O_5, nitrate radical (NO_3), HONO, HNO_4, Peroxyacetyl nitrate (PAN), organic nitrate (ONIT), NH_4^+ aerosol and NO_3^- aerosol) over China. The model, which has been widely used in previous studies for regional air quality and Nr deposition simulations[73–77], operates at a 30-km horizontal resolution and includes 30 vertical layers. In this study, the meteorological initial and boundary conditions were provided by the 1° × 1° Final analysis data from the National Centers for Environmental Prediction. The chemical initial and boundary conditions were derived from the CAM-Chem model[78]. The gas-phase chemistry used in the present study was based on the Carbon Bond Mechanism version Z mechanism[79]. The aerosol treatments in the model were represented by the Model for Simulating Aerosol Interactions and Chemistry (MOSAIC) aerosol module with eight aerosol size sections (that is, 0.0390625–0.078125, 0.078125–0.15625, 0.15625–0.3125, 0.3125–0.625, 0.625–1.25, 1.25–2.5, 2.5–5.0 and 5.0–10.0 μm in dry particle diameter)[39]. Following previous studies[80,81], we used the geometric mean diameter of the maximum and minimum particle sizes in each size stage to calculate the particle size distribution. On the basis of prior sampling research[80,82], the aerosols are primarily under dry conditions during sampling. Consequently, we excluded aerosol water content when computing aerosol size distributions.

The wet deposition processes of gases and aerosols were modelled using the standard approach, which includes both in-cloud and below-cloud scavenging[83]. To calculate the total wet deposition of nitrogen-containing aerosols, we aggregated all wet scavenging processes. This includes the wet removal of aerosols by resolved clouds and precipitation, the wet removal of aerosol precursor gases (HNO_3 for NO_3^- and NH_3 for NH_4^+) by resolved clouds/precipitation and the wet removal of precursor gases and aerosols by convective clouds/rain[77]. The dry deposition of gases was modelled following Wesely's scheme[84]. For the dry deposition of particles, we considered four size-dependent dry deposition parameterizations, detailed further in the study.

Surface properties, such as land-use type, notably influence aerosol dry deposition velocity[31,45]. Land-use types in China have undergone considerable changes over the past decades. The default land-use dataset in the WRF-Chem model, based on data from 1992, is outdated for our 2015 simulations over China (Supplementary Table 7). To address this, we replaced the default US Geological Survey land-use data in the WRF-Chem model with the more recent Global Land Cover 2015 dataset[85]. The detailed physical and chemical settings of the WRF-Chem model configurations are presented in Supplementary Table 8. The emissions data utilized in this study are described in Supplementary Text 5.

Particle size distribution

We considered two types of particle size distribution treatment in the atmospheric chemistry model. One is the standard model's particle size distributions, denoted as 'M_{size}'. The other one is the observation-constrained particle size distribution, denoted as 'O_{size}'. For the observation-constrained approach, we used observationally constrained particle sizes for NO_3^-, NH_4^+ and SO_4^{2-} aerosols under the three typical air pollution conditions (normal, lightly polluted and heavily polluted) in 2015 mentioned earlier. As the formation of NO_3^-, NH_4^+ and SO_4^{2-} aerosols in the atmosphere mutually influence each other[23,86], previous observations have shown similar size distribution patterns in the accumulation mode for these three aerosols[70,71]. Therefore, we constrained the size distribution of these aerosol species simultaneously.

In the O_{size} simulations, we first determined daily average $PM_{2.5}$ concentrations for all model grid cells using the WRF-Chem standard model (M_{size}_BS1995; 'Aerosol dry deposition mechanisms'). We then

classified air pollution conditions for each grid cell according to the daily average $PM_{2.5}$ concentration at the surface for each time step. On the basis of observational data ('Observations'), we constrained the size distributions of NO_3^-, NH_4^+ and SO_4^{2-} aerosols in the simulations according to different air pollution conditions. Specifically, the particle size distributions of these aerosols were set to modal sizes of 0.60 µm, 0.69 µm and 0.92 µm and geometric standard deviations of 1.8 µm, 1.95 µm and 1.94 µm, under normal, lightly polluted and heavily polluted days, respectively. Particles with diameters smaller than 2.5 µm are typically classified as 'fine,' whereas those larger than 2.5 µm are referred to as 'coarse'[35]. We focused on the particle size distribution of the fine mode, as secondary inorganic aerosols such as NH_4^+ and NO_3^- are predominantly found in smaller particle sizes[23,24,82]. Hence, we constrained the distributions of the three inorganic aerosol components within the first six bins of the MOSAIC model. During this process, we ensured that the total concentration of a certain aerosol component in these six size bins remained unchanged. We then used the observed particle size distribution to refine the distribution of aerosols within the different size segments. By doing so, we updated the aerosol concentrations for each size bin and calculated the subsequent dry deposition based on the revised particle size distribution. These constraints were applied for each grid cell.

Aerosol dry deposition mechanisms

In this study, we considered four dry deposition mechanisms for particulate matter in the WRF-Chem atmospheric chemistry model: 'BS1995', 'PE1992', 'Z2001' and 'E2020'. These mechanisms are based on aerosol dry deposition models from Binkowski and Shankar[42], Peters and Eiden[41], Zhang et al.[43] and Emerson et al.[31], respectively. The BS1995 mechanism is the default dry deposition mechanism for aerosols in the MOSAIC module of the WRF-Chem model[87]. PE1992 was once widely used, though it is no longer recommended. It remains an optional dry deposition scheme in the WRF-Chem model with the MOSAIC module. The Z2001 mechanism is extensively applied in various CTMs and ESMs, such as GEOS-Chem, CAMx, CESM-CAM5 and WRF-Chem model[44,88–90]. The E2020 mechanism is the newest particle dry deposition mechanism developed by Emerson et al., an observationally constrained parameterization recently introduced in GEOS-Chem[31].

These four particle dry deposition mechanisms simulate particle deposition rates using distinct approaches. In most CTMs, the dry deposition algorithms calculate the particle deposition velocity as a function of the particle size. Most particle dry deposition mechanisms in the current CTMs are derived from the trailblazing work of Slinn et al.[91–93]. Slinn et al. divided the boundary layer into two layers: the aerodynamic layer and the vegetation layer. The upper layer, from a certain reference height to the canopy top, is defined as the aerodynamic layer. The lower layer, which is from the top of the vegetation to the ground, is defined as the vegetation layer.

The dry deposition velocity of particles (V_d, m s^{-1}) is generally represented by the following equation:

$$V_d = V_g + \frac{1}{R_a + R_s} \quad (1)$$

in which, V_g is the gravitational settling velocity (m s^{-1}), which is present throughout the whole of the deposition process; R_a, the aerodynamic resistance (s m^{-1}), represents the resistance encountered by particles falling through the aerodynamic layer, specifically the resistance of particulate matter descending from a certain height to Earth's surface. This resistance is associated with airflow transport and turbulent mixing effects; R_s is the surface resistance (s m^{-1}), representing the resistance of particles in the vegetation layer. The surface resistance mainly contains the loss efficiency caused by three main physical processes: Brownian diffusion, interception and impaction and is corrected using the rebound coefficient. The surface resistance is expressed as below[31]:

$$R_s = \frac{1}{\varepsilon_0 u_* (E_B + E_{IM} + E_{IN}) R} \quad (2)$$

where ε_0 is the empirical coefficient (unitless); u_* is the friction velocity (m s^{-1}); E_B is the collection efficiency from Brownian diffusion (unitless), which refers to the random movement of particles in the atmosphere and non-convective diffusion; E_{IM} is the collection efficiency from impaction (unitless), which refers to the phenomenon that particles with high inertia, unable to move with the airflow and directly impact with the surface; E_{IN} is the collection efficiency from interception (unitless), which refers to the phenomenon that particles with low inertia flowing with the flow field are trapped within a distance from the collector less than the single-particle radius of the collector; R is the rebound correction factor of particles (unitless), which refers to the reduction of particles collected on the surface due to the rebound effect. Using different particle size distributions affects R_s because the three processes are size-dependent (Extended Data Table 1), leading to differences in dry deposition velocity calculations using different mechanisms.

The four particle dry deposition mechanisms employed in our study all utilize a resistance model similar to the one described above to calculate the dry deposition velocity of atmospheric particles. Each mechanism, however, differs in specific parameters and analytical approaches, detailed in Extended Data Table 1. The primary distinction among the four mechanisms mainly comes from the surface resistance, whereas the differences in gravitational settlement and aerodynamic resistance are relatively minor[52,94]. Notably, the E2020 mechanism, refined through extensive observations across various land-use types, is the most up to date and provides the most accurate method for quantifying atmospheric Nr deposition. Consequently, we tested and applied this latest mechanism to quantify atmospheric Nr deposition in China.

Simulation experiment design

To examine the effects of particle size distribution and dry deposition mechanisms on the particulate Nr deposition over China, eight WRF-Chem simulation experiments were conducted (Supplementary Table 9): M_{size}_BS1995, M_{size}_PE1992, M_{size}_Z2001, M_{size}_E2020, O_{size}_BS1995, O_{size}_PE1992, O_{size}_Z2001 and O_{size}_E2020. These simulations were set in the year 2015, primarily due to the availability of relevant observational data. Among the eight experiments, three key experiments (that is, M_{size}_BS1995, M_{size}_Z2001 and O_{size}_E2020) were conducted for 12 months, from January to December, with five days of model spin-up for each monthly simulation. These three experiments were selected because they represent typical results from previous studies: the default WRF-Chem setting, the default GEOS-Chem setting and the observation-constrained result from this study. The differences in the impact of particle size distribution and dry deposition mechanisms on Nr deposition were derived from these three experiments. The full 12-month Nr deposition results from these three experiments were used to drive the land surface model to evaluate the impact of nitrogen deposition on terrestrial carbon sinks.

Because WRF-Chem includes detailed atmospheric processes and achieves good simulation accuracy, the computation time and resource costs are considerable. To optimize computational efficiency, previous studies have simplified simulation durations by selecting representative months to estimate annual deposition fluxes[76,95,96]. Therefore, in this study, the remaining five simulation experiments were run for January, April, July and October to represent the four seasons. To validate this approach, we compared the annual totals of the four-month results from M_{size}_BS1995, M_{size}_Z2001 and O_{size}_E2020 to those using the full 12-month results. The results were highly consistent, with

a proportional coefficient of 3.1 across all three experiments. Consequently, we applied a factor of 3.1 to the deposition estimates for January, April, July and October to compute the annual total when we needed to analyse the differences across all eight experiments.

The dry deposition flux (F_i, μgN m^2 s^{-1}) of a specific particulate Nr species (i) in the WRF-Chem model was predicted by multiplying surface concentration (C_i, μgN m^{-3}) by the dry deposition velocity ($V_{d,i}$, m s^{-1}) of the species, as expressed by the following equation:

$$F_i = -C_i \times V_{d,i} \quad (3)$$

Land surface model simulations

We employed the state-of-the-art CLM5 model[97] to investigate the impact of Nr deposition on the terrestrial carbon sink in China. CLM5 is a process-based land surface model that describes the cycling of energy, water, momentum, carbon, nitrogen and other trace gases in terrestrial ecosystems. It has been widely applied in the area of the intersection of weather and climate with terrestrial processes, such as exploring the carbon and nitrogen cycle interactions and assessing ecosystems' response and vulnerability to climate change and disturbances[98]. Compared to previous versions, CLM5 incorporates notable improvements representing nitrogen cycling, including the implementation of flexible plant C:N ratios, accounting for carbon costs associated with nitrogen acquisition based on the Fixation and Uptake of Nitrogen model and optimizing leaf nitrogen content for photosynthesis[97]. The improvements in carbon and nitrogen cycling and coupling processes allow us to effectively evaluate how the terrestrial carbon cycle responds to Nr deposition changes.

We conducted several CLM5 simulation experiments over China from 1850 to 2014, with a resolution of 1.9° × 2.5°, following the method in published literature[75]. The simulations were forced with the Global Soil Wetness Project 3 version 1 climate reconstructions. Initially, we commenced the model spin-up process to achieve a steady state. During this phase, we maintained the atmospheric CO_2 concentration and land-cover data consistent with the year 1850, fixed nitrogen deposition at 1850 levels and set the climate forcing for the period of 1901–1920. Subsequently, we conducted historical simulations for the period of 1850–1900. Because the forcing data were available only from 1901 onwards, we used recycling climate forcings from 1901 to 1920 for the earlier simulations before 1900[99]. Incorporating other input data, we accounted for the rise in CO_2 concentration, increased Nr deposition and changes in land cover over time. Then, all simulations were run from 1901 to 2004, encompassing time-varying atmospheric CO_2 concentration, Nr deposition, land-cover data and climate forcings. Finally, we performed simulations from 2005 to 2014, employing atmospheric CO_2 concentration and land-cover data from transient datasets. For this 10-year period, following published literature[75], we varied Nr deposition fluxes in the model by substituting the default Nr deposition data with three distinct sets derived from WRF-Chem 2015 simulations: M_{size}_PS1995 (default settings in the WRF-Chem model), M_{size}_Z2001 (default settings in the GEOS-Chem model) and O_{size}_E2020 (settings constrained by observations). The ten-year averaged model results from 2005 to 2014 were used to analyse the terrestrial carbon sink budget. Following previous studies[65,75], NEP was selected as the indicator for the land carbon sink.

In the CLM model, land-use data is integrated using a nested subgrid hierarchy, where grid cells consist of multiple land units, columns and patches[97]. In contrast, WRF-Chem incorporates land-use data through interpolation[100]. Despite different processing methods, both models use land-use data derived from historical remote sensing data, ensuring consistency. To drive the CLM model with WRF-Chem Nr deposition data, we resampled the grid cells during the resolution conversion process to maintain consistency with the total Nr deposition. However, this process probably introduces some uncertainty in the flux distribution across adjacent grid cells. Additionally, the CLM model includes nitrogen fertilizer application data for both fertilizer and manure applications. Industrial fertilization is based on crop type, year and country, using fertilization rates from the Land Use Harmonization Version 2 dataset, whereas manure-based fertilization is applied uniformly at a rate of 2 gN m^{-2} yr^{-1} (ref. 101). Although efforts are underway to improve manure application representation, including transient application rates and N fluxes, these have not been included in the released version of CLM5[101]. To validate our terrestrial carbon uptake modelling, we employed NASA's Moderate Resolution Imaging Spectroradiometer (MODIS)/Terra NPP product, which has a spatial resolution of 0.1 degrees. Our comparison of CLM5 with the NPP product indicates that CLM5 demonstrates reliable accuracy in carbon cycle modelling, evidenced by a high R^2 value of 0.74 (Extended Data Fig. 4).

Data availability

The underlying data employed in this study are available from sources cited in the main text and Supplementary Information or are provided in Supplementary Data. The CMIP6 data are available at https://aims2.llnl.gov/search/cmip6/. The revised map database is available via GitHub at https://github.com/huangynj/NCL-Chinamap.

Code availability

The default WRF-Chem model source code is freely available at https://www2.mmm.ucar.edu/wrf/users/download/get_sources_new.php. The CLM5 model code is available via Github at https://github.com/ESCOMP/CTSM/releases.

References

69. Fu, Y. et al. Enhanced atmospheric nitrogen deposition at a rural site in northwest China from 2011 to 2018. *Atmos. Res.* **245**, 105071 (2020).
70. Huang, X. J. et al. Seasonal variation and secondary formation of size-segregated aerosol water-soluble inorganic ions during pollution episodes in Beijing. *Atmos. Res.* **168**, 70–79 (2016).
71. Yao, Q. et al. Seasonal variation and secondary formation of size-segregated aerosol water-soluble inorganic ions in a coast megacity of North China Plain. *Environ. Sci. Pollut. Res.* **27**, 26750–26762 (2020).
72. *China National Ambient Air Quality Standards*(GB 3095-2012) (Ministry of Environmental Protection of the People's Republic of China, 2012).
73. Shrivastava, M. et al. Urban pollution greatly enhances formation of natural aerosols over the Amazon rainforest. *Nat. Commun.* **10**, 1046 (2019).
74. Oikawa, P. Y. et al. Unusually high soil nitrogen oxide emissions influence air quality in a high-temperature agricultural region. *Nat. Commun.* **6**, 8753 (2015).
75. Liu, M. X. et al. Unexpected response of nitrogen deposition to nitrogen oxide controls and implications for land carbon sink. *Nat. Commun.* **13**, 3126 (2022).
76. Liu, M. X. et al. Ammonia emission control in China would mitigate haze pollution and nitrogen deposition, but worsen acid rain. *Proc. Natl Acad. Sci. USA* **116**, 7760–7765 (2019).
77. Ryu, Y. H. & Min, S. K. Improving wet and dry deposition of aerosols in WRF-Chem: updates to below-cloud scavenging and coarse-particle dry deposition. *J. Adv. Model. Earth Syst.* **14**, e2021MS002792 (2022).
78. Buchholz,R. R., Emmons, L. K., Tilmes, S. & The CESM2 Development Team. CESM2.1/CAM-chem instantaneous output forboundary conditions. Subset used with Lat: 10 to 60, Lon: 60 to 140, December 2014–December 2015. UCAR/NCAR -Atmospheric Chemistry Observations and Modeling Laboratory https://doi.org/10.5065/NMP7-EP60 (2019).

79. Zaveri, R. A. & Peters, L. K. A new lumped structure photochemical mechanism for large-scale applications. *J. Geophys. Res.: Atmos.* **104**, 30387–30415 (1999).
80. Su, J., Zhao, P. & Dong, Q. Chemical compositions and liquid water content of size-resolved aerosol in Beijing. *Aerosol Air Qual. Res.* **18**, 680–692 (2018).
81. Ding, X. et al. Long-range and regional transported size-resolved atmospheric aerosols during summertime in urban Shanghai. *Sci. Total Environ.* **583**, 334–343 (2017).
82. Zhao, P. S., Chen, Y. N. & Su, J. Size-resolved carbonaceous components and water-soluble ions measurements of ambient aerosol in Beijing. *J. Environ. Sci.* **54**, 298–313 (2017).
83. Easter, R. C. et al. MIRAGE: model description and evaluation of aerosols and trace gases. *J. Geophys. Res.: Atmos.* **109**, D20210 (2004).
84. Wesely, M. Parameterization of surface resistances to gaseous dry deposition in regional-scale numerical models. *Atmos. Environ.* **23**, 1293–1304 (1989).
85. Li, H. Q., Zhang, H. L., Mamtimin, A., Fan, S. Y. & Ju, C. X. A new land-use dataset for the Weather Research and Forecasting (WRF) model. *Atmosphere* **11**, 350 (2020).
86. Wang, Y., Zhang, Q., He, K., Zhang, Q. & Chai, L. Sulfate-nitrate-ammonium aerosols over China: response to 2000–2015 emission changes of sulfur dioxide, nitrogen oxides, and ammonia. *Atmos. Chem. Phys.* **13**, 2635–2652 (2013).
87. Peckham, S. E. et al. *WRF-Chem version 3.9.1.1 User's Guide* (NOAA, 2017).
88. Shu, Q., Koo, B., Yarwood, G. & Henderson, B. H. Strong influence of deposition and vertical mixing on secondary organic aerosol concentrations in CMAQ and CAMx. *Atmos. Environ.* **171**, 317–329 (2017).
89. Wu, M. X. et al. Impacts of aerosol dry deposition on black carbon spatial distributions and radiative effects in the Community Atmosphere Model CAM5. *J. Adv. Model. Earth Syst.* **10**, 1150–1171 (2018).
90. Timmermans, R. et al. Evaluation of modelled LOTOS-EUROS with observational based PM10 source attribution. *Atmos. Environ.: X* **14**, 100173 (2022).
91. Slinn, W. G. N. Predictions for particle deposition to vegetative canopies. *Atmos. Environ.* **16**, 1785–1794 (1982).
92. Slinn, S. A. & Slinn, W. G. N. Predictions for particle deposition on natural-waters. *Atmos. Environ.* **14**, 1013–1016 (1980).
93. Slinn, W. Some approximations for the wet and dry removal of particles and gases from the atmosphere. *Water Air Soil Pollut.* **7**, 513–543 (1977).
94. Bergametti, G. et al. Size-resolved dry deposition velocities of dust particles: in situ measurements and parameterizations testing. *J. Geophys. Res.: Atmos.* **123**, 11080–11099 (2018).
95. Xu, W. et al. Spatial–temporal patterns of inorganic nitrogen air concentrations and deposition in eastern China. *Atmos. Chem. Phys.* **18**, 10931–10954 (2018).
96. Zhang, Y., Yu, Q., Ma, W. & Chen, L. Atmospheric deposition of inorganic nitrogen to the eastern China seas and its implications to marine biogeochemistry. *J. Geophys. Res.: Atmos.* **115**, D00K10 (2010).
97. Lawrence, D. M. et al. The Community Land Model version 5: description of new features, benchmarking, and impact of forcing uncertainty. *J. Adv. Model. Earth Syst.* **11**, 4245–4287 (2019).
98. Davies-Barnard, T. et al. Nitrogen cycling in CMIP6 land surface models: progress and limitations. *Biogeosciences* **17**, 5129–5148 (2020).
99. Bonan, G. B. et al. Model structure and climate data uncertainty in historical simulations of the terrestrial carbon cycle (1850–2014). *Glob. Biogeochem. Cycles* **33**, 1310–1326 (2019).
100. Skamarock, W. C. *A Description of the Advanced Research WRF Version 3* NCAR technical note 475 (NCAR, 2008).
101. Lombardozzi, D. L. et al. Simulating agriculture in the Community Land Model version 5. *J. Geophys. Res.: Biogeosci.* **125**, e2019JG005529 (2020).
102. Wang, L., Wen, T.-X., Miao, H.-Y., Gao, W.-K. & Wang, Y.-S. Concentrations and size distributions of water-soluble inorganic ions in aerosol particles in Taiyuan, Shanxi. *Environ. Sci.* **37**, 3249–3257 (2016).
103. Wang, L. *Characteristics and Regional Distributions of Size-Segregated Water-Soluble Inorganic Ions in Atmospheric Particulate Matters in China*. PhD thesis, Univ. of Chinese Academy of Sciences (2017).

Acknowledgements

This study was funded by the National Natural Science Foundation of China (grant numbers 42476127, 42577530 and 42521004); China Postdoctoral Science Foundation (2022M720005); Beijing Natural Science Foundation (8244068) and Science and Technology Projects of Xizang Autonomous Region, China (XZ202501ZY0091), and was supported by the High-Performance Computing Platform of Peking University and in part through research cyberinfrastructure resources and services provided by the Partnership for an Advanced Computing Environment (PACE) at the Georgia Institute of Technology, Atlanta, Georgia, USA. We also thank the public instrument platform of the College of Urban and Environmental Sciences at Peking University. Maodian Liu is also supported by the Fundamental Research Funds for the Central Universities, Peking University (7100604874). Y.-H.R. was funded by the National Research Foundation of Korea (NRF) grant funded by the Korean Government (MSIT) (RS-2023-00274625). H.L. was funded by the National Natural Science Foundation of China (42275166). We thank Y. Huang (IAP/CAS) for providing the map database (https://github.com/huangynj/NCL-Chinamap.git).

Author contributions

Y.W., X.W., Maodian Liu and Q.Z. designed and led the research; X.W., Maodian Liu and Q.Z. acquired the funding needed to complete the study; Q.Z. and Maodian Liu performed the research and data collection; Y.-H.R. and Mingxu Liu contributed to the model configuration; H.L. contributed the updated land-use data; Y.W., Q.Z. and Maodian Liu made the data analysis and interpreted the results; Q.Z. and Maodian Liu wrote the original manuscript in close discussion with Y.W., S.W., J.L., S.T. and X.W. and all authors contributed to manuscript revision and completion.

Competing interests

The authors declare no competing interests.

Additional information

Extended data is available for this paper at https://doi.org/10.1038/s41561-025-01873-3.

Supplementary information The online version contains supplementary material available at https://doi.org/10.1038/s41561-025-01873-3.

Correspondence and requests for materials should be addressed to Yuhang Wang, Maodian Liu or Xuejun Wang.

Peer review information *Nature Geoscience* thanks Cheng Gong and the other, anonymous, reviewer(s) for their contribution to the peer review of this work. Primary Handling Editors: Camilla Brunello, Xujia Jiang and Carolina Ortiz Guerrero, in collaboration with the *Nature Geoscience* team.

https://doi.org/10.1038/s41561-025-01873-3

Extended Data Table 1 | Aerosol dry deposition schemes

Variable	PE1992	BS1995	Z2001	E2020
V_d	$V_d = V_g + \frac{1}{R_a+R_s}$	$V_d = V_g + \frac{1}{R_a+R_s+R_aR_sV_g}$	$V_d = V_g + \frac{1}{R_a+R_s+R_aR_sV_g}$	$V_d = V_g + \frac{1}{R_a+R_s+R_aR_sV_g}$
R_s	$R_s = \frac{1}{u_*(E_B+E_{IM}+E_{IN})R}$	$R_s = \frac{1}{u_*(E_B+E_{IM})}$	$R_s = \frac{1}{\varepsilon_0 u_*(E_B+E_{IM}+E_{IN})R}$	$R_s = \frac{1}{\varepsilon_0 u_*(E_B+E_{IM}+E_{IN})R}$
E_B	$E_B = Sc^{-\frac{2}{3}}$	$E_B = Sc^{-\frac{2}{3}}$	$E_B = Sc^{-\gamma}$ $\gamma \in [0.50, 0.58]$	$E_B = 0.2 * Sc^{-\frac{2}{3}}$
E_{IM}	$E_{IM} = (\frac{St}{0.8+St})^2$	$E_{IM} = 10^{-\frac{3}{St}}$	$E_{IM} = (\frac{St}{\alpha+St})^2$	$E_{IM} = 0.4 * (\frac{St}{\alpha+St})^{1.7}$
E_{IN}	$E_{IN} = \frac{(0.00116+0.0061z_0)d_p}{1.414*10^{-7}}$		$E_{IN} = \frac{1}{2}(\frac{d_p}{A})^2$ (vegetated surfaces) $E_{IN} = 0$(smooth surfaces)	$E_{IN} = 2.5 * (\frac{d_p}{A})^{0.8}$ (vegetated surfaces) $E_{IN} = 0$(smooth surfaces)
R	$R = e^{-2\sqrt{St}}$		$R = e^{-\sqrt{St}}$	$R = e^{-\sqrt{St}}$
St	$St = \frac{\rho_p d_p^2}{9\mu d_c} u$	$St = \frac{u_*^2 V_g}{gv}$	$St = \frac{V_g u_*}{gA}$ (vegetated surfaces) $St = \frac{V_g u_*^2}{gv}$ (smooth surfaces)	$St = \frac{V_g u_*}{gA}$ (vegetated surfaces) $St = \frac{V_g u_*^2}{gv}$ (smooth surfaces)
V_g	$\frac{\rho_p d_p^2 g C_c}{18\mu}$	$\frac{\rho_p d_p^2 g C_c}{18\mu}$	$\frac{\rho_p d_p^2 g C_c}{18\mu}$	$\frac{\rho_p d_p^2 g C_c}{18\mu}$
S_c	$\frac{v}{D}$	$\frac{v}{D}$	$\frac{v}{D}$	$\frac{v}{D}$
Reference	41	42	43	31

The physical meaning of the main parameters in the Table: V_d is the dry deposition velocity; R_s is the surface resistance; E_B is the collection efficiency from Brownian diffusion; E_{IM} is the collection efficiency from impaction; E_{IN} is the collection efficiency from interception; R is the bounce correction factor; St is the Stokes number; V_g is the gravitational settling velocity; C_c is the Cunningham correction factor; R_a is the aerodynamic resistance; ε_0 is the coefficient; u_* is the friction velocity; Sc is the Schmidt number; u is the horizontal wind speed; d_p is the particle diameter of the particulate matter; d_c is the diameter of the obstacle; μ is the aerodynamic viscosity; ρ_p is the density of the particulate matter; A refers to the characteristic radius of collectors; v represents the kinematic viscosity of air; D is the Brownian diffusivity of particles, which is related to the particle diameter.

https://doi.org/10.1038/s41561-025-01873-3

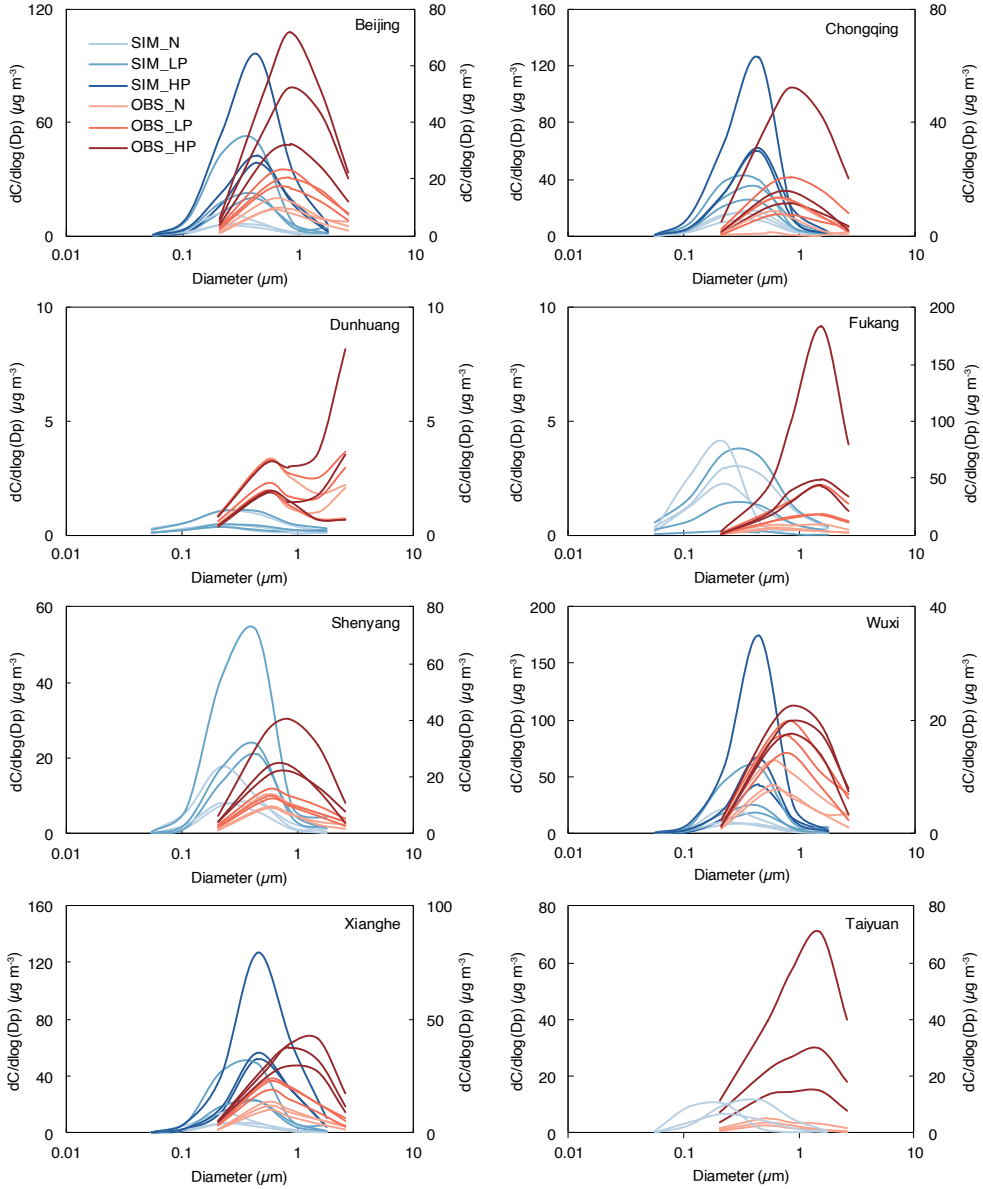

Extended Data Fig. 1 | Observed particle size distributions of NO_3^-, NH_4^+, and SO_4^{2-} aerosols under different air pollution conditions in China. The blue curves, ranging from light to dark, represent simulated results with pollution levels increasing from low to high, corresponding to the left y-axis. Similarly, the red curves, ranging from light to dark, depict observed results with increasing pollution levels from low to high, corresponding to the right y-axis. 'SIM' means simulations. 'OBS' means observations. 'N' means normal days. 'LP' means lightly polluted days. 'HP' means heavily polluted days. Daily air quality levels were classified based on average daily $PM_{2.5}$ values. Some cities did not have heavily polluted days during the simulation period, resulting in the absence of some locations in SIM_HP figures. The observations here are obtained from previous publications[102,103].

https://doi.org/10.1038/s41561-025-01873-3

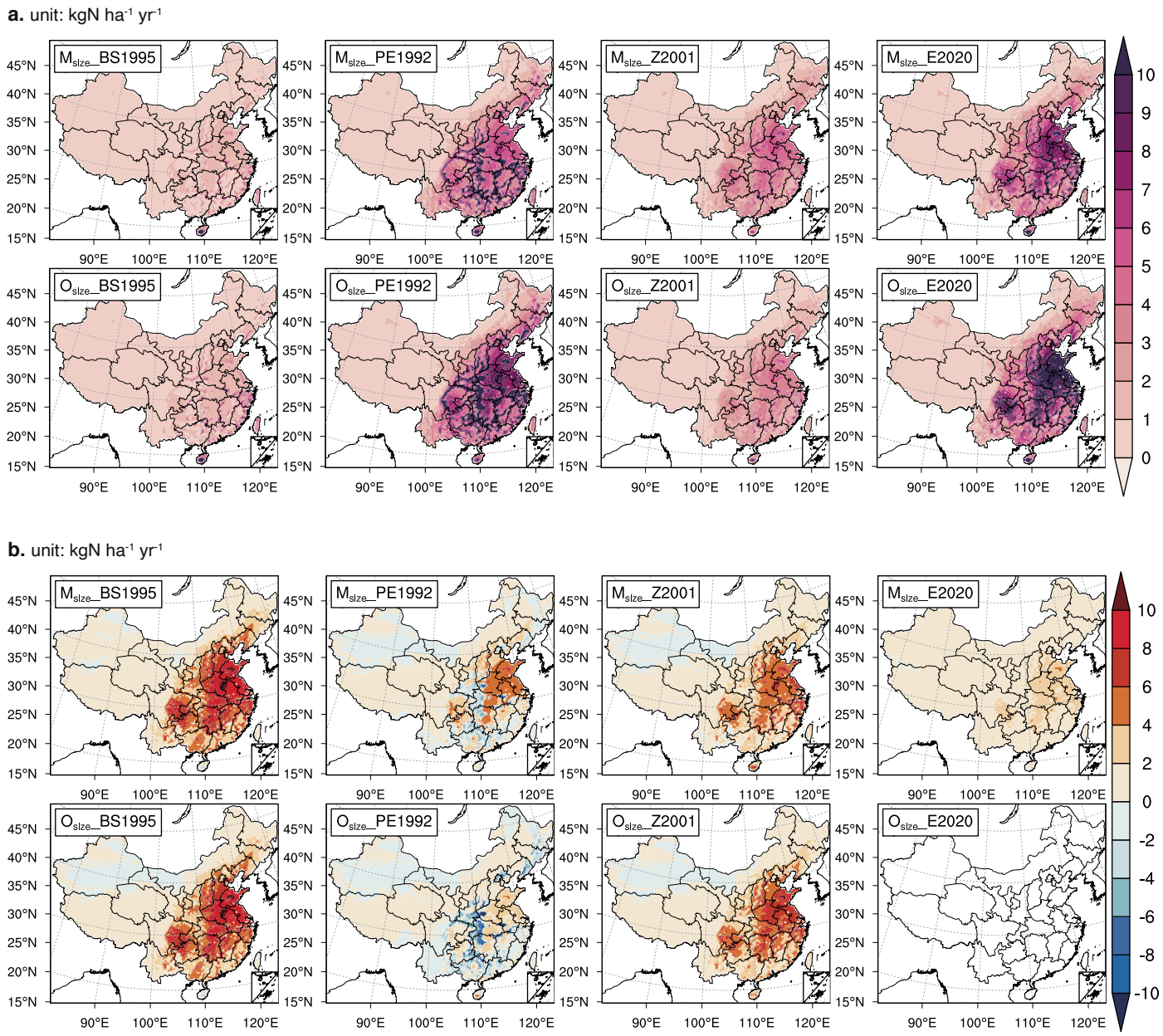

Extended Data Fig. 2 | Changes in particulate nitrogen dry deposition over China constrained by observed particle size and new deposition mechanisms. The spatial distribution of total particulate nitrogen dry deposition over China from the eight simulation experiments (**a**) and change in total particulate nitrogen dry deposition of the observation-derived experiment (O_{size}_E2020) compared with each other simulation experiment (**b**). Maps based on the original NCAR Command Language (NCL) map framework with updated boundary information derived from the National Catalogue Service for Geographic Information of China (http://www.webmap.cn/commres.do?method=result100W).

https://doi.org/10.1038/s41561-025-01873-3

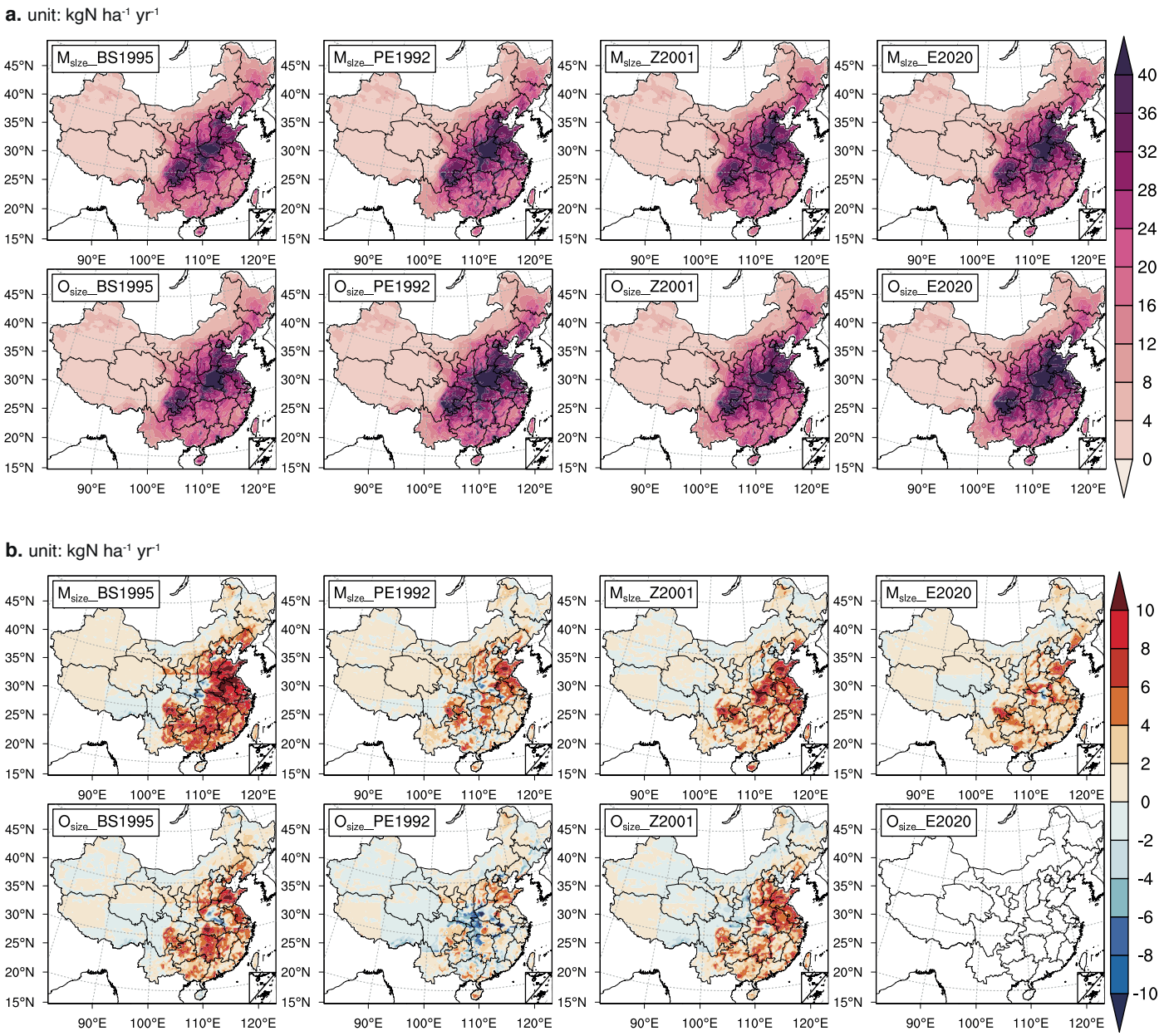

Extended Data Fig. 3 | Changes in total nitrogen deposition over China constrained by observed particle size and new deposition mechanisms. The spatial distribution of total nitrogen deposition over China from the eight simulation experiments (**a**) and change in total nitrogen deposition of the observation-derived experiment (O_{size}_E2020) compared with each other simulation experiment (**b**). Maps based on the original NCAR Command Language (NCL) map framework with updated boundary information derived from the National Catalogue Service for Geographic Information of China (http://www.webmap.cn/commres.do?method=result100W).

https://doi.org/10.1038/s41561-025-01873-3

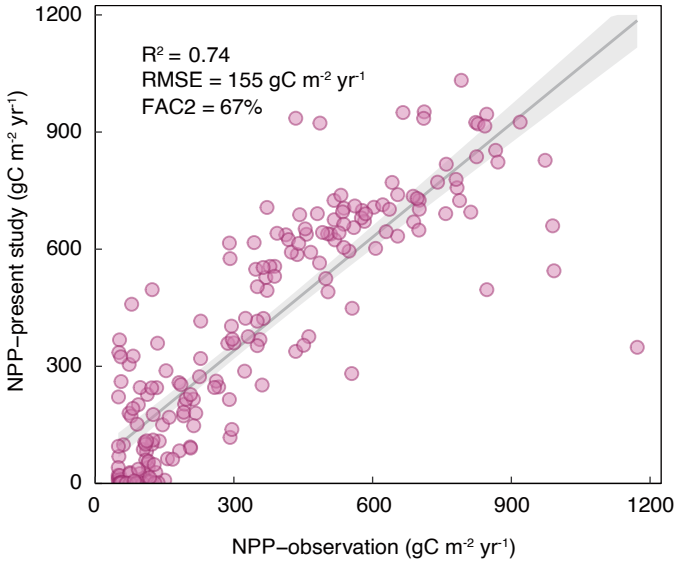

Extended Data Fig. 4 | The comparison of net primary productivity (NPP) between simulations with the NASA NPP observations across China. The gray line indicates the linear regression fit (mean estimate), and the gray shaded area denotes the 95% confidence interval for that regression line. Statistical metrics including R-squared ($R^2 = 0.74$), root-mean-square deviation (RMSE = 155 gC m^{-2} yr^{-1}) and fraction of simulation within a factor of two (FAC2 = 67%) are presented.